Little known impacts on the accuracy of the Gibson method

Petr SEVCIK — *OSC a.s.*, *Czech Republic*, *E-mail: petr.sevcik@osc.cz*

Vladimír HABÁN — *Brno University of Technology*, *Czech Republic*, *haban@fme.vutbr.cz*

Daniel HIMR — *Brno University of Technology*, *Czech Republic*, *himr@fme.vutbr.cz*

Abstract

The focus of hydraulic experts dealing with refinement of the pressure-time method is mainly focused on hydraulic phenomena in pipelines. But there exist also other phenomena, mainly caused by parasitic features of sensors and tested equipment, which have similar weight as the first mentioned. These phenomena are usually not taken into consideration by flow rate evaluation.

The first part of this paper presents example of theoretical work - simulation of penstock irregularities impact on correct calculation. The simulation was performed in CFD software and obtained flow rate and pressure were used to determine the penstock factor.

The second part brings description of following impacts comparable with above mentioned hydraulic phenomena:

- Experimental determination of pressure sensors parasitic features like slow signal stabilization within accuracy class which can cause error due by long integration.
- Change of guide vanes leakage during machine deceleration for units without main intake valve (MIV) and bad condition of guide vanes, MIV, bypass etc.

Description of these hardware phenomena is based on long time experience with Gibson method.

1. CFD determination of cone penstock factor

The chapter presents the use and possibilities of determining correction factors when using the pressure-time method sometimes called Gibson's method (GM) for measuring flow in large water structures with the penstock of non-constant cross-section. According to the IEC 41 standard, it is possible to use GM only in the case of a direct penstock of constant cross-section, but many penstocks deviate from these conditions, thus it is necessary to determine the penstock factor in another way. For this determination of the penstock factor, it is possible to use simple mathematical relationships and integration along the length of the penstock. Another possibility is a procedure using CFD modelling of unsteady flow in the penstock and determining the penstock factor based on the CFD results. This procedure is usable for penstock of an arbitrary shape. The procedure based on CFD computation is described in presented paper.

1.1. Basic derivation

Following conical pipe is considered, see Fig. 1.

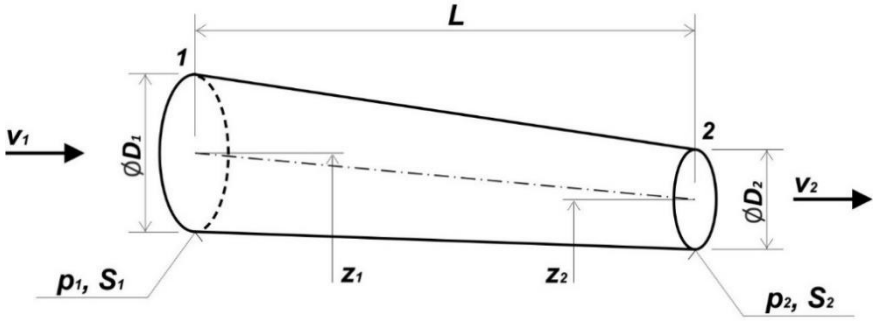

Fig. 1

It is possible to come out from the Bernoulli equation, where integral covers an unsteady case.

$$\frac{p_1}{\rho}+\frac{v_1^2}{2}+g\cdot z_1=\frac{p_2}{\rho}+\frac{v_2^2}{2}+g\cdot z_2+Y_{z12}+\int_1^2 a_t dL,$$

where Y_{z12}, stands for energy loss. Introducing pressure difference

$$\Delta p=p_2-p_1+\rho\cdot g\cdot(z_2-z_1)$$

allows rearranging Bernoulli equation into different shape

$$\Delta p = -\Delta p_z - \rho \frac{\partial Q}{\partial t} \int_1^2 \frac{dL}{S} - \rho \frac{Q^2}{2} \left(\frac{1}{S_2^2} - \frac{1}{S_1^2} \right),$$

where flow rate is introduced and Δp_z represents pressure loss, which can be described as

$$\Delta p_z = R \cdot |Q(t)| \cdot Q(t).$$

According to IEC 41 standard [1], penstock factor can be computed

$$P_f = \int_{L_1}^{L_2} \frac{l}{S} dl = \int_0^L \frac{x}{S} dx.$$

Final equation for flow rate computation is

$$\rho P_f \frac{\partial Q}{\partial t} = -R \cdot |Q(t)| \cdot Q(t) - \Delta p$$

$$\frac{\partial Q}{\partial t} = -\frac{1}{P_f \rho} \left(\Delta p + R \cdot |Q(t)| \cdot Q(t) \right), \quad (1)$$

where Δp is measured pressure difference, which is modified with respect to static head. So, flow rate as function of time can be obtained as the solution.

1.2. Cone penstock factor

The cone is very often placed upstream the turbine and it is not possible to measure pressure upstream the cone, because the penstock is embedded in the concrete. The considered cone is drawn in the Fig. 2

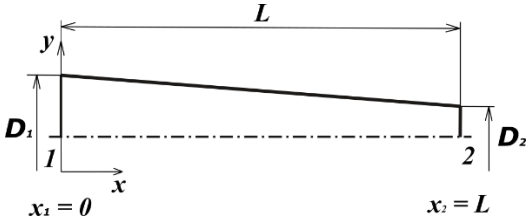

Fig. 2

Following equations describe diameter and cross-section.

$$D = D_1 + \frac{D_2 - D_1}{L} x,$$

$$S = \frac{\pi \cdot D^2}{4} = \frac{\pi}{4} \left(D_1 + \frac{D_2 - D_1}{L} x \right)^2.$$

Thus the penstock factor is

$$P_f = \int_0^L \frac{l}{S} dx = \int_0^L \frac{l}{\frac{\pi}{4} \left(D_1 + \frac{D_2 - D_1}{L} x \right)^2} dx = \frac{4}{\pi} \int_0^L \frac{l}{\left(D_1 + \frac{D_2 - D_1}{L} x \right)^2} dx,$$

$$P_f = \frac{4}{\pi} \frac{L}{D_1 \cdot D_2} = \frac{L}{\pi \cdot R_1 \cdot R_2}. \quad (2)$$

1.3. CFD model

CFD model is shown in the Fig. 3. Diameters were chosen with respect to HPP Lipno $D_1 = 4.5$ m, $D_2 = 2.5$ m and cone length L is 7.6 m.

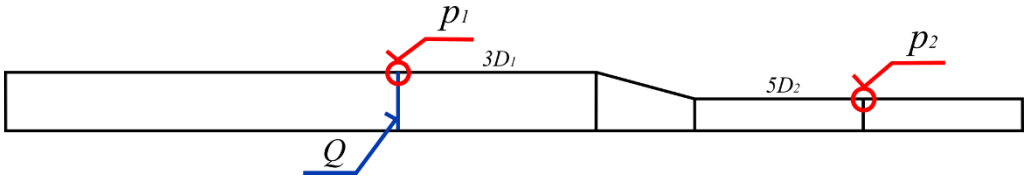

Fig. 3

The pressure was monitored in place 3xD1 upstream the cone and 3xD2 downstream the cone. The computational domain was 5xD longer upstream and downstream the measurement to prevent negative influence of boundary conditions.

Velocity inlet condition was defined in three time periods. $v = v_0$ for time $T = (0; T_0)$, $v = 0$ for $T > T_0 + T_1$ and

$$v = v_0 \frac{1}{2}\left\{1 + \cos\left[\frac{\pi}{T_1}(t - T_0)\right]\right\}; \quad T \in \langle T_0; T_1 \rangle$$

Obtained flow rate is shown in the following figure. Initial flow velocity is $v_0 = 5$m/s. The closured starts at time $T_0 = 5$ s and ends within time $T_1 = 5$ s. Following figure Fig. 4 contains also measured pressure difference.

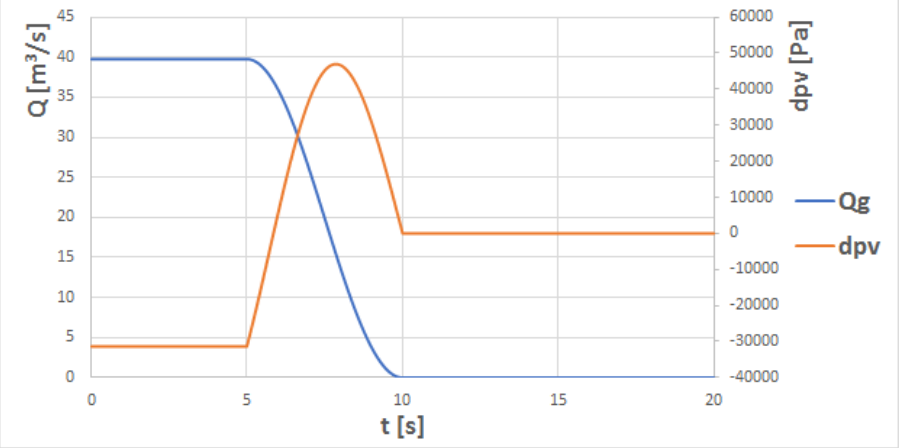

Fig. 4

It is possible to determine the penstock factor from CFD results (pressure difference and flow rate) according to IEC 41. It is a numerical solution of Equation (1). The value of penstock factor of the conical part is obtained after subtraction of penstock factor of direct parts. Following table shows theoretical penstock factor of the cone by Equation (2), which is compared with CFD solution for different closing time. More details on solution can be found in [2].

Tab. 1: Comparison of cone penstock factor based on geometrical dimensions with CFD determination

$P_{f,\,theor}$ [m^{-1}]	T_1 [s]	P_{f_CFD} [m^{-1}]	*deviation* [%]
0.860144	5	0.861835	0.196569
	4	0.868241	0.941326
	3	0.868664	0.990579
	2	0.863499	0.390038
	1	0.864538	0.510798

2. Impact of sensors shortcomings

The inspiration for investigating the behavior of sensors under increasing and decreasing pressure was our own experience with the calibration of pressure sensors as well as calibration protocols from accredited calibration laboratories. Example of the different output signal during the up and down series is presented in Fig. 5. Therefore the simple test device was prepared by OSC staff to check the repeatability of pressure values in condition similar by Gibson test – see Fig. 6. A set of two 2.5 MPa pressure sensors, a BEAMEX calibrator and a pressure pump was connected to a ϕ6 mm hose with a 22 m of water column terminated by a special 100 mm diameter compensating bottle with a free water level.

2.1. Description of test

The test procedure was as follows:

- The static pressure created by the water column was scanned by both pressure sensors for several minutes.
- Then the valve was closed and the pressure was increased by a pressure pump.
- The valve was opened after approx. 30 s and the pressure returned back to the previous value created by the water column.

Record of such experiment is presented in Fig. 7. Three tests were performed, two of them were evaluated as presented below. (The first one was a device functionality test.)

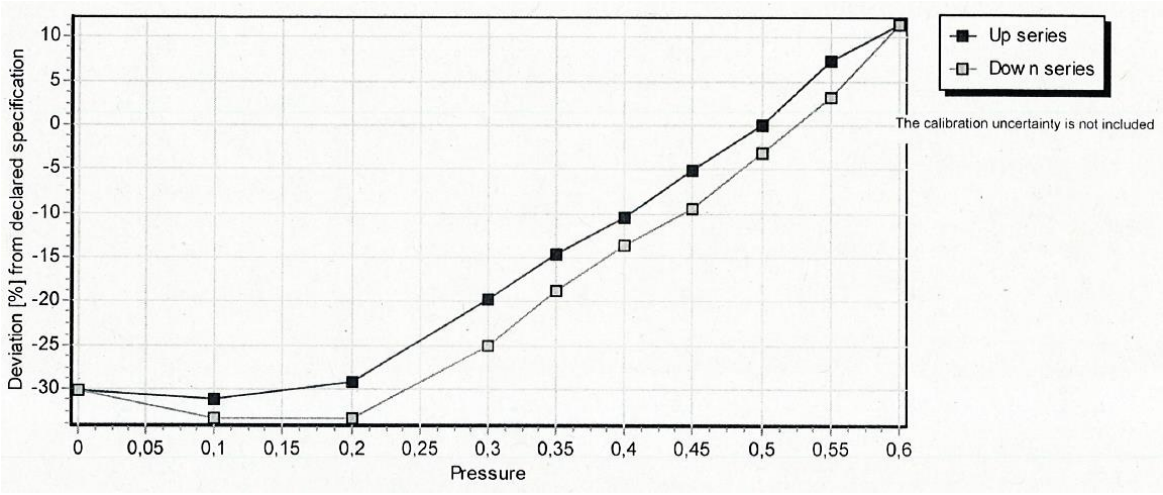

Fig. 5: Graphical presentation of up and down calibration series of sensor 2.5 MPa made by accredited laboratory

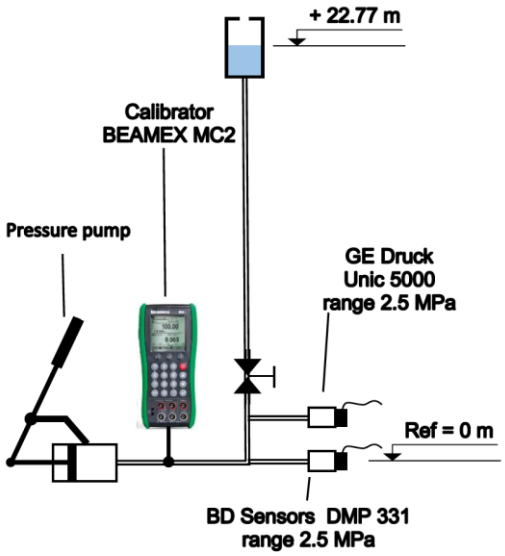

Fig. 6: Simple device for simulating of condition during Gibson test

Fig. 7: Record of simulated water hammer change

2.2. Tests evaluation

Following two types of evaluation were performed:

a) Comparison of average pressure from time intervals lasting approx. 30 s before and after the pressure change. As can be seen from the results presented in Tab. 2, both sensors have very good repeatability according to the mentioned criterion. The difference between the mean values before and after the pressure increase is significantly smaller than the tolerance corresponding to the accuracy class 0.2.

Tab. 2: Comparison of average pressure values before and after simulation of water hammer

Test No.	$p_{BD\ before}$	$p_{BD\ after}$	Δp_{BD}	Δp_{BD}	Δp_{BD}	$p_{GE\ before}$	$p_{GE\ after}$	Δp_{GE}	Δp_{GE}	Δp_{GE}
	kPa	kPa	kPa	% FS	% WH	kPa	kPa	kPa	% FS	% WH
2	223.354	223.354	0.000	0.00%	0.00%	219.618	219.548	0.070	0.00%	0.05%
3	223.309	223.301	0.008	0.00%	0.01%	219.525	219.475	0.050	0.00%	0.04%

Explanation of terms:

p_{BD}, p_{GE} - pressure measured by sensors BD Sensors, GE Druck

subscript $_{before}$ - values scanned before water hammer simulation

subscript $_{after}$ - values scanned after water hammer simulation

$\Delta p_{subscript}$ [kPa] - difference $p_{XXbefore} - p_{XXafter}$

$\Delta p_{subscript}$ [% FS] - difference $p_{XXbefore} - p_{XXafter}$ as percentage of sensor full scale (2.5 MPa)

$\Delta p_{subscript}$ [% WH] - difference $p_{XXbefore} - p_{XXafter}$ as percentage of water hammer overpressure during turbine shut down (HPP Lipno – Δp_{GIB} = 140 kPa, H = 160 m)

b) Pressure gradient after pressure increasing. The detail of the pressure stabilization in test No. 2 after the simulated water hammer is shown in Fig. 8. The output of pressure p_{GE} has an increasing tendency with trend 11 Pa/s after pressure drop. Output signal of sensor p_{BD} is constant as evident from the record. Integration of such growing value can cause a problem with evaluation of Gibson flow rate as presented below. Contrary to expectations, however, when the experiment was repeated again, a similar phenomenon did not occur (test No. 3.).

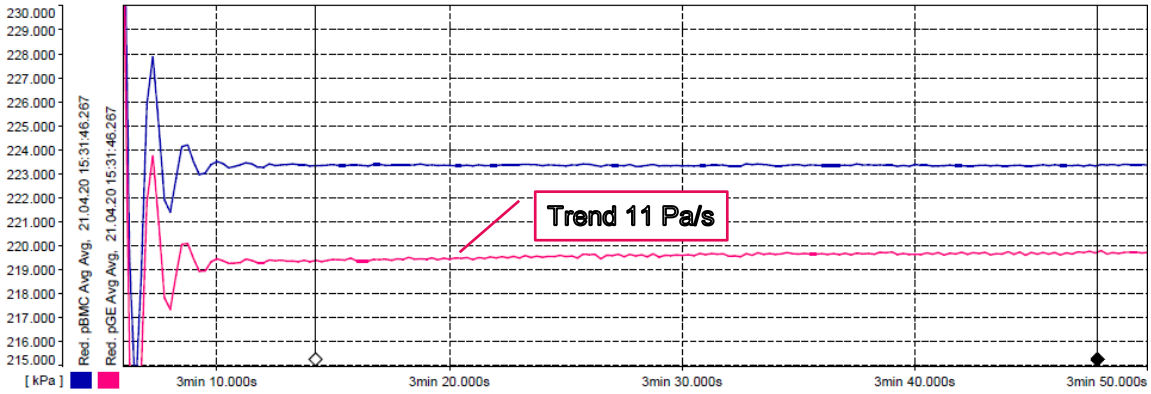

Fig. 8: Detail of growing p_{GE} value after water hammer simulation

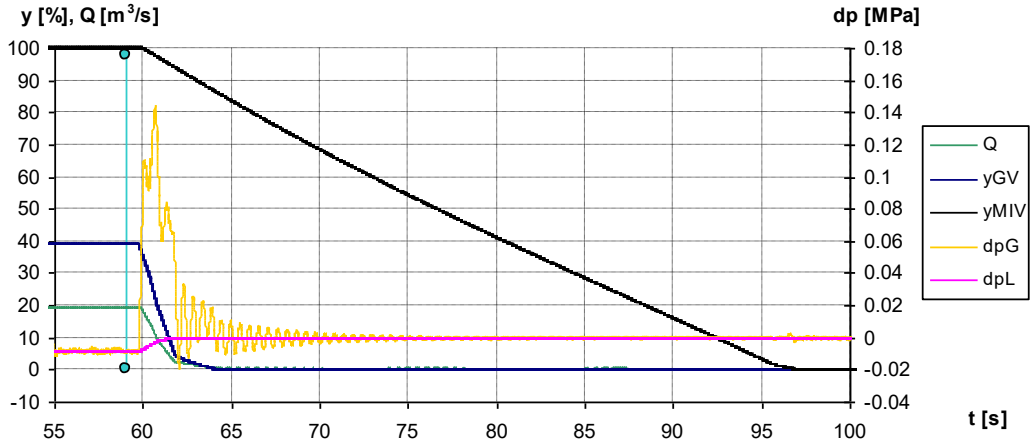

Fig. 9: Typical waveform of signals for Gibson flow evaluation (HPP Lipno, partial load)

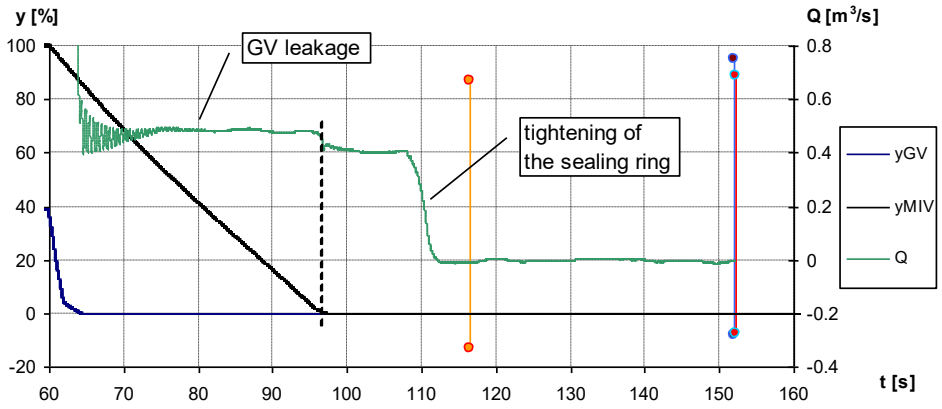

Fig. 10: Detail of the flow wave during and after MIV closure

Typical waveforms from the recording and calculation of the Gibson flow rate are shown in Fig. 9 and Fig. 10. The pressure signal in this case had the correct stabilization waveform after the unit fast shut down - similar to p_{BD} in above mentioned OSC experiment.

Two additional calculations were performed again with data modification in the stable part from the 110th s of the record. A linear rising pressure with a trend of 11 Pa/s was added to the steady pressure after MIV closure. This simplification was chosen instead of a true exponential curve as sufficient to demonstrate the effect on the resulting flow rate. Results are available in following Fig. 11, Fig. 12 and Tab. 3.

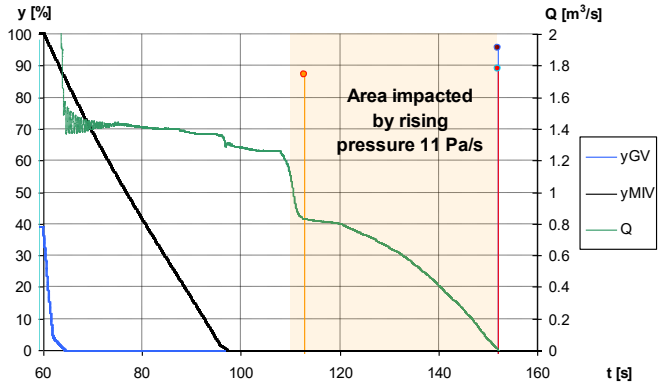

Fig. 11: Detail of termination of integration with rising pressure of 11 Pa/s during stabilization with original zero determination and integration interval

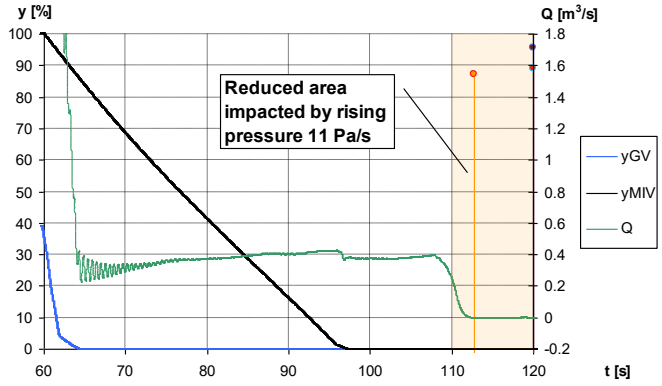

Fig. 12: Detail of termination of integration performed using procedure as described in [3]

Tab. 3: Comparison of the flow rate based on the correct signal and the signal affected by long stabilization

Case	Q [m³/s]	ΔQ	
Original measurement with correct pressure stabilisation	19.448	-	
Rising pressure during stabilisation, original zero and end of integration	20.468	5.25%	
Rising pressure during stabilisation, evaluation procedure according to [3]	19.256	-0.99%	

3. Conclusion

The possibility of applying Gibson method (pressure - time) as it is described in the currently valid standard [1] is gradually being extended to penstocks including bends, conical parts and other irregularities. The society of water energy experts is dedicated to refining calculation algorithms for these cases. One of such examples is presented in chap. 1.

But similar or bigger impact on measurement uncertainty can have a sensors shortcomings which are difficult to detect. As presented in Chap. 2, the sensors meet all the parameters corresponding with their accuracy class. There was found a slow stabilization of output signal of one of tested sensors and just only in one test. But the integration of small rising signal causes a significant error of final flow rate. Our experience confirms occasional cases of strange flow course after closing the MIV, when the flow should be zero.

However, the shortcomings of the tested machine can also have similar manifestations, especially if it is an older, worn-out device:

- Bad mechanical condition of the guide vanes requiring a long time to eliminate clearances.
- Bad condition of MIV bypass or relief valves where the flow rate has a varying value.

Following measures should be implemented to recognize reason of strange flow wave shape close to end of integration:

- To record the guide vane, MIV and other valves positions. It is then possible to recognize the individual phases of the closing procedure and compare the calculated flow wave with real possible values.
- The result of the integration of the increasing pressure difference is the flow rate pattern close to a parabola. It is better to repeat the test for identical unit setting in this case.
- It is possible to eliminate partially the calculation error using evaluation procedure as described in [3].

References

[1] Standard IEC 41: "*Field acceptance tests to determine the hydraulic performance of hydraulic turbines, storage pumps and pump turbines*", standard issued by CEI, 1991.

[2] Hrubý E, *Pressure-time method for determination of the flow rate in the hydro power plants* (Brno, Brno University of Technology), 2017.

[3] Ševčík P., "*Exact zero determination and integration termination for pressure – time method*", in Conference IGHEM 2014, Itajuba, Brasil.

[4] Ramdal J. ,Jonsson P., Nielsen T., "*Influence from bends on a pressure-time measurement*", in 25th IAHR Symposium on Hydraulic Machinery and Systems, 2010, Brno, Czech Republic

Acknowledgement

This paper was supported by Smart Energy Systems ERA-NET project 108786, Digitalization of water supply infrastructure to optimize the Water-Energy Nexus (DIWIEN).